PREPRINT 459

NOVEMBER 2016

High Order Unfitted Finite Element Methods for Interface Problems and PDEs on Surfaces

Christoph Lehrenfeld and Arnold Reusken

Institut für Geometrie und Praktische Mathematik
Templergraben 55, 52062 Aachen, Germany

Christoph Lehrenfeld
Institut für Numerische und Angewandte Mathematik, Lotzestr. 16-18, D-37083 Göttingen, Germany,
e-mail: lehrenfeld@math.uni-goettingen.de
Arnold Reusken
Institut für Geometrie und Praktische Mathematik, RWTH Aachen University, D-52056 Aachen, Germany,
e-mail: reusken@igpm.rwth-aachen.de

High Order Unfitted Finite Element Methods for Interface Problems and PDEs on Surfaces

Christoph Lehrenfeld and Arnold Reusken

1 Introduction

In this contribution we treat a special class of recently developed unfitted finite element methods for the discretization of mass and surfactant transport equations in incompressible two-phase flow problems. For the two-phase flow problem we restrict to a *sharp interface* model for the fluid dynamics, which consists of the Navier-Stokes equations for the bulk fluids with an interfacial surface tension force term in the momentum equation. In case of solute transport this Navier-Stokes equation is coupled with a convection-diffusion equation. If surfactants are present, a convection-diffusion equation on the (evolving) interface is used for modeling the surfactant transport. We refer to, e.g., [19] for a derivation and discussion of these models. In this contribution we do not consider the Navier-Stokes equations for the fluid dynamics and restrict to the transport equations for solute and surfactants which will are introduced below.
A key difficulty in the numerical simulation of two-phase flow problems is an accurate numerical approximation of the interface. For this different techniques have been developed in the literature, e.g., volume of fluid (VOF) and level set methods. In this contribution we restrict to the level set (LS) method. Furthermore, as discretization method for the mass and surfactant equations we restrict to finite element methods (FEM). In such a setting with a (standard) LS method for interface capturing, the underlying computational grids are typically *not* fitted to the (evolving) interface and thus one needs special finite element methods that can deal with such *un*fitted triangulations. Recently, significant progress has been made in the

Christoph Lehrenfeld
Institut für Numerische und Angewandte Mathematik, Lotzestr. 16-18, D-37083 Göttingen, Germany, e-mail: lehrenfeld@math.uni-goettingen.de

Arnold Reusken
Institut für Geometrie und Praktische Mathematik, RWTH Aachen University, D-52056 Aachen, Germany, e-mail: reusken@igpm.rwth-aachen.de

construction, analysis and application of methods of this kind, see for instance the papers [6, 7, 13, 18, 20, 40] and the references therein. In the literature different names for such unfitted FEM for the discretization of the solute transport equation are also used, namely extended FEM (XFEM) and CutFEM. Unfitted FEM are also used for the discretization of PDEs on (evolving) manifolds, e.g., [39] and the references therein. While most of the work on unfitted discretizations has been on piecewise linear (unfitted) finite elements, many unfitted discretizations have a natural extension to higher order finite element spaces, see for instance [1, 23, 35, 44]. Nevertheless, new techniques are required to obtain also higher order accuracy when errors due to the geometry approximation are also considered.

In this contribution we present the main results on unfitted FEM obtained in the Priority Program 1506. More detailed treatments of these results are given in the papers [26, 27, 28, 29, 30, 31, 32, 33, 34, 39, 41] and [14]. We outline our main new results at the end of this chapter, cf. section 5.

The structure of the paper is as follows. In section 2 we treat higher order unfitted FEM for elliptic interface problems. In section 3 higher order unfitted FEM for elliptic partial differential equations on (evolving) surfaces are discussed. These general techniques have rather straightforward applications to the mass and surfactant equations that occur in two-phase flows. This is addressed in section 4. Finally, in section 5 we outline our main nuew results and discuss some topics which we consider to be of interest for further study.

2 Unfitted FEM for interface problems

Below, in section 2.1 we first restrict to a model interface problem with a *stationary* interface and then in section 2.2 extend the approach to *evolving* interfaces. The discretizations of the interface problems are based on the unfitted Nitsche method from the seminal paper [20] and extend it to higher order methods and evolving domains. The key ideas of the new finite element method are explained, optimal theoretical error bounds are discussed and results of a numerical example, which illustrates the behavior of the method, are included. The results in this section are based on [28, 29, 32, 33, 34].

2.1 Model elliptic problem with a stationary interface

On a bounded connected polygonal domain $\Omega \subset \mathbb{R}^d$, $d = 2,3$, we consider the model interface problem

$$-\mathrm{div}(\alpha_i \nabla u) = f_i \quad \text{in } \Omega_i,\ i = 1,2, \tag{1a}$$

$$[\![-\alpha \nabla u]\!]_\Gamma \cdot \mathbf{n}_\Gamma = 0, \quad [\![u]\!]_\Gamma = 0 \quad \text{on } \Gamma, \tag{1b}$$

$$u = 0 \quad \text{on } \partial\Omega. \tag{1c}$$

Here, $\Omega_1 \cup \Omega_2 = \Omega$ is a nonoverlapping partitioning of the domain, $\Gamma = \overline{\Omega}_1 \cap \overline{\Omega}_2$ is the interface, $[\![\cdot]\!]_\Gamma$ denotes the usual jump operator across Γ and $\mathbf{n}_\Gamma$ denotes the unit normal at Γ pointing from Ω_1 into Ω_2. f_i, $i = 1,2$ are domain-wise described sources. In the remainder we will also use the source term f on Ω which we define as $f|_{\Omega_i} = f_i$, $i = 1,2$. The diffusion coefficient α is assumed to be piecewise constant, i.e. it has a constant value $\alpha_i > 0$ on each sub-domain Ω_i. In the following we use the notation $u_i = u|_{\Omega_i}$, $i = 1,2$.

The first interface condition in (1b) results from the conservation of mass principle while the second condition ensures continuity of the solution across the interface. Later, in section 2.2 we replace the second condition $[\![u]\!] = 0$ with the more general – and in the context of two-phase flow applications more relevant – *Henry jump condition* $[\![\beta u]\!] = 0$ where β is strictly positive and piecewise constant. In contrast to the problem considered in section 2.2, a problem as in (1) with the condition $[\![u]\!]_\Gamma = 0$ replaced by the Henry condition $[\![\beta u]\!] = 0$, $\beta_1 \neq \beta_2$ (which has a jump discontinuity in the solution u), can be transformed to a problem of the form of (1) using the variable $w = \beta u$. As the problem with the interface condition $[\![u]\!] = 0$ is a standard model problem in the literature we consider only this condition in the remainder of this section. We however note that the methods presented in the following can also be applied to the more general Henry condition, cf. [29, 48].

The weak formulation of the problem (1) is as follows: determine $u \in H_0^1(\Omega)$ such that

$$\int_\Omega \alpha \nabla u \cdot \nabla v \, dx = \int_\Omega f v \, dx \quad \text{for all } v \in H_0^1(\Omega). \tag{2}$$

We assume simplicial triangulations of Ω which are *not* fitted to Γ. Furthermore, the interface is characterized as the zero level of a given level set function ϕ. The numerically challenging aspect of the problem in (1) stems from the fact that the diffusion coefficient α can be discontinuous across the *unfitted* interface. Hence, the solution can have discontinuities in the gradient which are located inside individual elements. This lack of regularity of the solution introduces difficulties in the accurate approximation. Standard piecewise polynomial finite element spaces are no longer appropriate and lead to sub-optimal results, especially when aiming at higher order convergence. To overcome the approximation problem special finite element spaces are typically designed. Below, in section 2.1.1 we consider an established choice, an unfitted finite element space as it is used in XFEM or CutFEM discretizations. One drawback of the application of this kind of finite element space is that none of the interface conditions in (1b) can easily be implemented in the finite element space as a n essential condition. A suitable finite element method with these adapted finite element spaces needs a variational formulation which includes the interface conditions at least in a weak sense. Another important difficulty in the numerical treatment of (1) is in the accurate handling of geometries, which are only implicitly defined through level set functions. Especially the realization of integrals which

have discontinuous integrands is difficult, for instance the weak Laplacian in (2). Especially for higher order methods solving this task with sufficient accuracy is a challenging task. In the next section we introduce an unfitted finite element methods which addresses all the aforementioned problems. Afterwards, in sections 2.1.2 and 2.1.3 we give a priori error bounds and numerical results. We restrict to the pure diffusion problem (1). In [29] a variant of the unfitted FEM, based on a streamline diffusion stabilization technique, is treated which is suitable for the discretization of elliptic convection dominated interface problems.

2.1.1 An unfitted finite element method

In [28] a new approach has been introduced to obtain higher order accurate approximations of domain and surface integrals of implicitly described geometries. The fundamental idea is the introduction of a parametric mapping Θ_h of the underlying mesh from a geometrical reference configuration to a final configuration.

Let $\mathscr{T}$ denote the simplicial triangulation of Ω and V_h^k denote the standard finite element space of continuous piecewise polynomials up to degree k. The nodal interpolation operator in V_h^k is denoted by I_k. It is assumed that a high order accurate finite element approximation ϕ_h of the level set funcion ϕ is known. Based on its piecewise linear interpolation $\hat{\phi}_h = I_1\phi_h$ the reference configuration with the subdomains $\Omega_i^{\text{lin}} = \{\hat{\phi}_h \lessgtr 0\},\ i = 1,2$ and the interface $\Gamma^{\text{lin}} = \{\hat{\phi}_h = 0\}$ is defined. For this reference configuration a robust and accurate realization of numerical integration is fairly simple. Inside each element the interface and the subdomains are convex polytopes for which quadrature rules can easily be obtained, cf. (among others) [27, Chapter 4], [36], [37, Chapter 5]. This kind of strategy is used in many simulation codes that are based on unfitted finite elements, e.g. [6, 8, 11, 17, 45]. Note that this piecewise planar approximation of the geometry is only second order accurate and thus its application is limited to low order methods. However, with a suitable choice of the parametric mapping Θ_h this approximation can be improved to a higher order accurate one. In [28] we introduced such a mapping which is easy to construct and realizes the mapping from the reference geometries to a higher order accurate approximation. A sketch is given in Fig. 1.

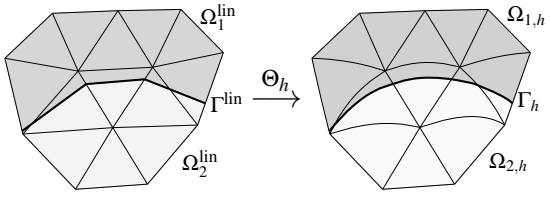

Fig. 1 Basic idea of the method in [28]: The zero level Γ^{lin} of the piecewise linear interpolation $\hat{\phi}_h$ is mapped approximately to the implicit interface $\{\phi_h = 0\}$ using a mesh transformation Θ_h.

The discretization approach consists of two steps. First, a (higher order) finite element discretization is constructed with respect to the reference configuration. Afterwards, applying the transformation Θ_h to this space and the geometries in the variational formulation results in a new unfitted finite element discretization with an accurate treatment of the geometries. The mapping renders the finite element

spaces *isoparametric finite element spaces*. As usual in isoparametric finite element discretizations, volume and interface integrals that occur in the implementation of the method can be formulated in terms of integrals on the reference configuration, i.e. on convex polytopes. This allows to reuse the established strategy for numerical integration discussed before.

We outline the construction of Θ_h, cf. [28] for more details. For ease of presentation we assume quasi-uniformity of the mesh, s.t. h denotes a characteristic mesh size with $h \sim h_T := \mathrm{diam}(T),\ T \in \mathscr{T}$. All elements in the triangulation $\mathscr{T}$ which are cut by Γ^{lin} are collected in the set $\mathscr{T}^\Gamma := \{T \in \mathscr{T}, T \cap \Gamma^{\mathrm{lin}} \neq \emptyset\}$. The corresponding domain is $\Omega^\Gamma := \{x \in T, T \in \mathscr{T}^\Gamma\}$ and the restriction of the finite element space to Ω^Γ is $V_h^k(\Omega^\Gamma) = V_h^k|_{\Omega^\Gamma}$. The extended set which includes all direct neighbors to elements in $\mathscr{T}^\Gamma$ is $\mathscr{T}_+^\Gamma := \{T \in \mathscr{T}, \mathrm{meas}_{d-1}(T \cap \Omega^\Gamma) \neq 0\}$ with the corresponding domain $\Omega_+^\Gamma := \{x \in T, T \in \mathscr{T}^\Gamma\}$.

For the isoparametric mapping Θ_h we first introduce a mapping Ψ_h on Ω^Γ which may be discontinuous, $\Psi_h \in C(\mathscr{T}^\Gamma)^d$ with $C(\mathscr{T}^\Gamma) = \bigoplus_{T \in \mathscr{T}^\Gamma} C(T)$. Then, we use a projection $P_h : C(\mathscr{T}^\Gamma)^d \to (V_h^k)^d$ to obtain a globally continuous mapping $\Theta_h := P_h\Psi_h$. Note that this ensures that Θ_h is a finite element (vector) function.

For the construction of Ψ_h we use the "search direction" $G_h(x) = \nabla\phi_h(x),\ x \in T \in \mathscr{T}^\Gamma$ which is a good approximation to $\nabla\phi$. Note that the latter coincides with the normal direction at the interface Γ. Other options for the search direction G_h are discussed in [28].

Let $\mathscr{E}_T\phi_h$ be the polynomial extension of $\phi_h|_T$. We define a function d_h as follows: $d_h(x)$ is the (in absolute value) smallest number such that

$$\mathscr{E}_T\phi_h(x + d_h(x)G_h(x)) = \hat{\phi}_h(x), \quad \text{for } x \in T \in \mathscr{T}^\Gamma. \tag{3}$$

Hence, at $x \in T$, the scalar function $d_h(x)$ is a steplength in the direction $G_h(x)$ such that the value of $\mathscr{E}_T\phi_h$ at $x + d_h(x)G_h(x)$ coincides with $\hat{\phi}_h(x)$. This function has the property $d_h(x_i) = 0$ for all *vertices* x_i of $T \in \mathscr{T}^\Gamma$. Given the function $d_hG_h \in C(\mathscr{T}^\Gamma)^d$ we define

$$\Psi_h(x) := x + d_h(x)G_h(x) \quad \text{for } x \in \Omega^\Gamma,\ \ \Theta_h := P_h\Psi_h = \mathrm{id} + Q_h(d_hG_h). \tag{4}$$

Here $Q_h := Q_h^2Q_h^1$ where Q_h^1 ensures continuity in Ω^Γ, $Q_h^1 : C(\mathscr{T}^\Gamma)^d \to V_h^k(\Omega^\Gamma)^d$ and $Q_h^2 : C(\Omega^\Gamma)^d \to C(\Omega)^d$ realizes the continuous transition to zero in $\Omega_+^\Gamma \setminus \Omega^\Gamma$, cf. the sketch in Fig. 2. Note that since $\Psi_h(x_i) = \Theta_h(x_i) = x_i$ for all *vertices* x_i, we have $\Psi_h = \Theta_h = \mathrm{id}$ for $k = 1$ in which case the mesh remains unchanged. For the projection operator Q_h^1 we consider a simple quasi-interpolation which averages function values across element interfaces, cf. also [43, Eqs.(25)-(26)] and [12]. For Q_h^2 we consider an operator which keeps the degrees of freedom in $\mathscr{T}^\Gamma$ unchanged and sets the remaining degrees of freedom to zero. For details on the projection P_h we refer to [28] and [32].

Remark 1. The mapping Θ_h should be a bijection on Ω and the transformed simplices $\Theta_h(T)$, $T \in \mathscr{T}$, should have some shape regularity property. One important result in [32] is that $\|D\Theta_h - \mathrm{id}\|_{\infty,T} \lesssim h$, i.e. for sufficiently small mesh sizes the

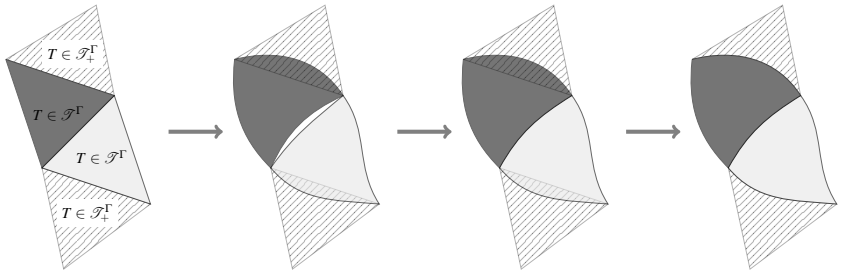

Fig. 2 Construction steps of the transformation Θ_h. In the first step, Ψ_h (only in Ω^Γ, pointwise, discontinuous across element interfaces) is constructed. In a second step, the discontinuities are removed through averaging (only in Ω^Γ). Finally, a continuous extension to the exterior is realized.

transformation becomes an arbitrary small perturbation to the identity and shape regularity of $\Theta(\mathscr{T})$ is inherited from the shape regularity of $\mathscr{T}$, cf. [32] for details. In cases where h is not sufficiently small to guarantee shape regularity the transformation has to be adapted. We refer to [28] for a possible way to achieve this.

We now define the isoparametric Nitsche unfitted FEM as a transformed version of the original Nitsche unfitted FE discretization [20] with respect to the interface approximation $\Gamma_h = \Theta_h(\Gamma^{\mathrm{lin}})$. We introduce some further notation. The standard unfitted space w.r.t. Γ^{lin} is denoted by

$$V_h^\Gamma := V_h^k{}_{|\Omega_1^{\mathrm{lin}}} \oplus V_h^k{}_{|\Omega_2^{\mathrm{lin}}}. \tag{5}$$

In the literature, a finite element method based on such a space is often called CutFEM, cf. [6] or extended FEM (XFEM), cf. [2, 13, 46]. To simplify the notation we do not explicitly express the polynomial degree k in V_h^Γ. The isoparametric unfitted FE space is defined as

$$V_{h,\Theta}^\Gamma := \{\, v_h \circ \Theta_h^{-1} \mid v_h \in V_h^\Gamma \,\} = \{\, \tilde{v}_h \mid \tilde{v}_h \circ \Theta_h \in V_h^\Gamma \,\}. \tag{6}$$

Based on this space we formulate a discretization of (1) using the unfitted Nitsche technique [20] with $\Gamma_h = \Theta_h(\Gamma^{\mathrm{lin}})$ and $\Omega_{i,h} = \Theta_h(\Omega_i^{\mathrm{lin}})$ as numerical approximation of the geometries: determine $u_h \in V_{h,\Theta}^\Gamma$ such that

$$A_h(u_h, v_h) := a_h(u_h, v_h) + N_h(u_h, v_h) = f_h(v_h) \quad \text{for all } v_h \in V_{h,\Theta}^\Gamma \tag{7}$$

with the bilinear forms

$$a_h(u,v) := \sum_{i=1}^{2} \alpha_i \int_{\Omega_{i,h}} \nabla u \cdot \nabla v dx, \tag{8a}$$

$$N_h(u,v) := N_h^c(u,v) + N_h^c(v,u) + N_h^s(u,v), \tag{8b}$$

$$N_h^c(u,v) := \int_{\Gamma_h} \{\!\{-\alpha \nabla v\}\!\} \cdot \mathbf{n}_{\Gamma_h} \, [\![u]\!] ds, \quad N_h^s(u,v) := \bar{\alpha} \frac{\lambda}{h} \int_{\Gamma_h} [\![u]\!][\![v]\!] ds, \tag{8c}$$

for $u, v \in V_{h,\Theta}^{\Gamma} + V_{\mathrm{reg},h}$ with $V_{\mathrm{reg},h} := H^1(\Omega) \cap H^2(\Omega_{1,h} \cup \Omega_{1,h})$.

Here, $\mathbf{n}_{\Gamma_h}$ denotes the outer normal of $\Omega_{1,h}$ and $\bar{\alpha} = \frac{1}{2}(\alpha_1 + \alpha_2)$ the mean diffusion coefficient. For the averaging operator $\{\!\{\cdot\}\!\}$ there are different possibilities. We use $\{\!\{w\}\!\} := \kappa_1 w_{|\Omega_{1,h}} + \kappa_2 w_{|\Omega_{2,h}}$ with a "Heaviside" choice where $\kappa_1 = 1$ if $|T_1| > \frac{1}{2}|T|$ and $\kappa_1 = 0$ if $|T_1| \leq \frac{1}{2}|T|$, $\kappa_2 = 1 - \kappa_1$. Here, $T_i = T \cap \Omega_i^{\mathrm{lin}}$, i.e. the cut configuration on the undeformed mesh is used. This choice in the averaging renders the scheme in (7) stable (for sufficiently large λ) for arbitrary polynomial degrees k, independent of the cut position of Γ, cf. [32, Lemma 5.1]. A different choice for the averaging which also results in a stable scheme is $\kappa_i = |T_i|/|T|$.

In order to define the right-hand side functional f_h we first assume that the source term $f_i : \Omega_i \to \mathbb{R}$ in (1a) is (smoothly) extended to $\Omega_{i,h}$, such that $f_i = f_{i,h}$ on Ω_i holds. This extension is denoted by $f_{i,h}$. We define

$$f_h(v) := \sum_{i=1,2} \int_{\Omega_{i,h}} f_{i,h} v dx, \quad v \in V_{h,\Theta}^{\Gamma} + V_{\mathrm{reg},h}. \tag{9}$$

We define f_h on Ω by $f_{h|\Omega_{i,h}} := f_{i,h}$, $i = 1,2$.

For the implementation of this method, in the integrals we apply a transformation of variables $y := \Theta_h^{-1}(x)$. For example, the bilinear form $a_h(u,v)$ then results in

$$a_h(u,v) := \sum_{i=1,2} \alpha_i \int_{\Omega_i^{\mathrm{lin}}} D\Theta_h^{-T} \nabla u \cdot D\Theta_h^{-T} \nabla v \, \det(D\Theta_h) \, dy. \tag{10}$$

Based on this transformation the implementation of integrals is carried out as for the case of the piecewise planar interface Γ^{lin}. The additional variable coefficients $D\Theta_h^{-T}$, $\det(D\Theta_h)$ are easily and efficiently computable using the property that Θ_h is a finite element (vector) function.

2.1.2 Optimal order error bound

Optimal discretization error bounds, both in the H^1- and L^2-norm, for the isoparametric unfitted FEM presented above are derived in [32, 33]. We only present the H^1-norm error bound. We assume that the approximation $\phi_h \in V_h^k$ of the level set function ϕ satisfies the error estimate

$$\max_{T \in \mathcal{T}} |\phi_h - \phi|_{m,\infty,T \cap U} \lesssim h^{k+1-m}, \quad 0 \leq m \leq k+1. \tag{11}$$

Here $|\cdot|_{m,\infty,T\cap U}$ denotes the usual semi-norm on the Sobolev space $W^{m,\infty}(T\cap U)$. Here and in the remainder we use the notation $\lesssim$, which denotes an inequality with a constant that is independent of h and of how the interface Γ intersects the triangulation $\mathscr{T}$. This constant may depend on ϕ and on the diffusion coefficient α, cf. (1a). A main theorem proved in [32] is the following. In the theorem we use a certain piecewise smooth function u^e, which is smooth on the subdomain approximations $\Omega_{i,h}$, $i=1,2$, and defined by a smooth extension of $u_{|\Omega_i}$ (cf. [32] for details).

Theorem 1. *Let u be the solution of* (1) *and $u_h \in V_{h,\Theta}^{\Gamma}$ the solution of* (7)*. We assume that $u \in H^{3,\infty}(\Omega_1\cup\Omega_2)$ if $k=2$, $u\in H^{k+1}(\Omega_1\cup\Omega_2)$ if $k\geq 3$, and $f\in H^{1,\infty}(\Omega_1\cup\Omega_2)$. Furthermore the data extension f_h satisfies the condition $\|f_h\|_{H^{1,\infty}(\Omega_{1,h}\cup\Omega_{2,h})} \lesssim \|f\|_{H^{1,\infty}(\Omega_1\cup\Omega_2)}$. Then the following holds:*

$$|u^e-u_h|_{H^1(\Omega_{i,h}\cup\Omega_{i,h})} \lesssim h^k\big(S(u)+\|f\|_{H^{1,\infty}(\Omega_1\cup\Omega_2)}\big)$$

with

$$S(u) := \begin{cases} \|u\|_{H^{3,\infty}(\Omega_1\cup\Omega_2)} & \text{if } k=2,\\ \|u\|_{H^{k+1}(\Omega_1\cup\Omega_2)} & \text{if } k\geq 3. \end{cases}$$

Hence, the method has the optimal h^k error bound in the H^1-norm, under almost optimal smoothness assumptions on u.

2.1.3 Results of numerical experiments

We give a numerical example to illustrate the performance of the previously introduced method. On the domain $\Omega=[-1.5,1.5]^2$ we prescribe the interface Γ by the level set function $\phi(x)=\|x\|_4-1$ where $\|x\|_4$ denotes the usual 4-norm on $\mathbb{R}^d$, $\Gamma=\{\phi(x)=0\}$. The interface is a smoothed square, c.f. the sketch in Fig. 3, the level set function ϕ is equivalent to a signed distance function. The diffusion parameters are taken as $(\alpha_1,\alpha_2)=(1,2)$, Dirichlet boundary data and right-hand side term f are chosen such that the solution is $u(x)=u_1(x)=1+\frac{\pi}{2}-\sqrt{2}\cdot\cos(\frac{\pi}{4}\|x\|_4^4)$ for $x\in\Omega_1$ and $u(x)=u_2(x)=\frac{\pi}{2}\|x\|_4$ for $x\in\Omega_2$. The solution is continuous across the interface, but has a kink at the interface, $u_1|_\Gamma=u_2|_\Gamma$ and $\alpha_1\nabla u_1\cdot\mathbf{n}_\Gamma=\alpha_2\nabla u_2\cdot\mathbf{n}_\Gamma$.

Based on a finite element approximation ϕ_h of ϕ which is obtained by higher order interpolation and the search direction $G_h=\nabla\phi_h$, we construct the mapping Θ_h as in (4). Starting from an initial simplicial mesh which resolves the interface sufficiently well such that we have shape regularity of the mesh after transformation with Θ_h, we repeatedly apply uniform refinements. The stabilization parameter in Nitsche's method is chosen as $\lambda=20\cdot k^2$.

In Fig. 3 the convergence results of the error u^e-u_h in the H^1 semi-norm for polynomial degrees $k=1,2,..,5$ are shown. Here, u^e is the natural extension of the solution to the discrete domains $\Omega_{i,h}$. We observe optimal order of convergence. For details on this numerical example we refer to [32]. We note that optimal order, i.e. $\mathscr{O}(h^{k+1})$ convergence for the error is also observed in the L^2 norm. These results confirm the error analyses in [32] (H^1 norm) and [33] (L^2 norm).

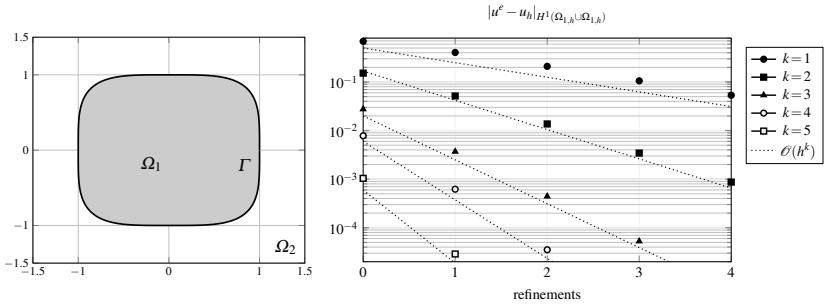

Fig. 3 Geometrical configuration and convergence results for the example in section 2.1.3.

Remark 2 (Dominating convection). In many applications, especially in two-phase flows, problems of the form (1) with an additional dominating convection term $\mathbf{w} \cdot \nabla u$ are relevant where $\mathbf{w}$ is the convecting flow field. In this case additional stabilization becomes necessary for the unfitted discretization introduced before. In [29] we derived and analysed a discretization which combines Streamline Diffusion stabilization with an unfitted finite element formulation for piecewise linears for the case of an elliptic interface problem with dominating convection.

Remark 3 (Conditioning stiffness matrix). A disadvantage of the type of unfitted finite element method presented above is the fact that the stiffness matrix can be extremely ill-conditioned. In particular this condition number depends not only on the mesh size h, but also on how the interface intersects the triangulation $\mathscr{T}$. This topic is addressed in [34] for the case of *linear* finite elements. An additive subspace preconditioner is introduced which is optimal in the sense that the resulting condition number is independent of *both* the mesh size h *and* the interface position. Furthermore it is shown that already the simple diagonal scaling of the stiffness matrix results in a condition number that is bounded by ch^{-2}, with a constant c that does not depend on the location of the interface.

2.2 Model parabolic problem with an evolving interface

We consider a mass transport problem with an *evolving* interface $\Gamma(t)$ which extends the previously considered model problem by adding convection and a temporal evolution of the concentration *and* the interface. We assume a given sufficiently smooth velocity field $\mathbf{w}$, with $\operatorname{div} \mathbf{w} = 0$, and assume that the transport of the interface is determined by this velocity field, in the sense that $V_\Gamma = \mathbf{w} \cdot \mathbf{n}_\Gamma$ holds. Here V_Γ is the normal velocity of the interface. We consider a standard model which describes the transport of a solute in a two-phase flow problem. In strong formulation this model is as follows:

$$\frac{\partial u}{\partial t} + \mathbf{w}\cdot\nabla u - \operatorname{div}(\alpha\nabla u) = f \quad \text{in } \Omega_i(t),\ i=1,2,\ t\in[0,T], \tag{12a}$$

$$[\![-\alpha\nabla u]\!]_\Gamma \cdot \mathbf{n}_\Gamma = 0, \quad [\![\beta u]\!]_\Gamma = 0 \quad \text{on } \Gamma, \tag{12b}$$

$$u(\cdot,0) = u_0 \quad \text{in } \Omega_i(0),\ i=1,2, \tag{12c}$$

$$u(\cdot,t) = 0 \quad \text{on } \partial\Omega,\ t\in[0,T]. \tag{12d}$$

In (12a) we have standard parabolic convection-diffusion equations in the two subdomains Ω_1 and Ω_2. The coefficients α, β are assumed to be piecewise constant. We note that in contrast to the problem treated in section 2.1.1 we now consider the general case $\alpha_1 \neq \alpha_2$ *and* $\beta_1 \neq \beta_2$. The second relation is the so-called *Henry condition*, cf. [21, 51, 50, 5, 4] and describes a jump discontinuity at the interface due to different solubilities within the respective fluid phases. Hence, the solution u is *discontinuous across the evolving interface*. In this section we treat an unfitted finite element method for this problem, introduced and analyzed in [30]. The method is based on a well-posed *space-time weak formulation* of (12) (which we do not present here). Compared to the unfitted finite element method presented in section 2.1.1 there are two important differences. Firstly, we restrict to *linear* finite elements and a *linear* interface reconstruction, i.e., we do not use an isoparametric mapping (for getting a higher order approximation). Hence, the best we can obtain is a second order method. Secondly, we treat the evolution by using a *space-time* finite element approach. We will introduce an unfitted space-time FEM and combine this with a space-time Nitsche technique. The method and results that we present are from [30]. From the error analysis, cf. section 2.2.2, it follows that the method is second order is space *and* time. We are not aware of any other Eulerian type discretization method for this class of parabolic interface problems which has a guaranteed (i.e., based on a-priori error bounds) second order convergence.

2.2.1 An unfitted FEM

The space-time unfitted FEM that we introduce in this section has the form of a variational problem in a certain space-time finite element space. The same space is used for both trial and test functions. We introduce the method for the case of piecewise *bilinear* space-time functions (linear in space and linear in time). In Remark 5 we comment on generalizations. We introduce notation. The space-time domain is denoted by $Q = \Omega \times (0,T] \subset \mathbb{R}^{d+1}$. A partitioning of the time interval is given by $0 = t_0 < t_1 < \ldots < t_N = T$, with a uniform time step $\Delta t = T/N$. This assumption of a uniform time step is made to simplify the presentation, but is not essential for the method. Corresponding to each time interval $I_n := (t_{n-1}, t_n]$ we assume a given shape regular simplicial triangulation $\mathscr{T}_n$ of the spatial domain Ω. In general this triangulation is *not fitted* to the interface $\Gamma(t)$. In this section we assume that the implicit geometries can be handled without introducing additional errors, cf. remark 4 below for the general case where geometries have to be approximated in order to obtain a realization of the discretization.

The triangulation $\mathscr{T}_n$ may vary with n. Let V_n be the finite element space of continuous piecewise linear functions on $\mathscr{T}_n$ with zero boundary values on $\partial\Omega$. The spatial mesh size parameter corresponding to V_n is denoted by h_n. Corresponding space-time finite element spaces on the time slab $Q^n := \Omega \times I_n$ are given by

$$W_n := \{\, v : Q^n \to \mathbb{R} \mid v(x,t) = \phi_0(x) + t\phi_1(x),\ \ \phi_0, \phi_1 \in V_n \,\} \tag{13a}$$

$$W := \{\, v : Q \to \mathbb{R} \mid v_{|Q^n} \in W_n \,\}. \tag{13b}$$

In the time slab Q^n we define the subdomains $Q_i^n := \cup_{t\in I_n} \Omega_i(t)$, $i = 1,2$, and also $Q_i := \cup_{1\le n\le N} Q_i^n = \cup_{0<t\le T} \Omega_i(t)$, $i = 1,2$. We will also use the notation $v_i := v|_{Q_i}$. The space-time *unfitted* FE spaces are given by

$$W_n^\Gamma := W_n|_{Q_1^n} \oplus W_n|_{Q_2^n} \tag{14a}$$

$$W^{\Gamma_*} := \{\, v : Q \to \mathbb{R} \mid v_{|Q^n} \in W_n^\Gamma \,\} = W|_{Q_1} \oplus W|_{Q_2}. \tag{14b}$$

The symbol Γ_*^n denotes the space-time interface in Q^n, i.e., $\Gamma_*^n := \cup_{t\in I_n} \Gamma(t)$, and $\Gamma_* := \cup_{1\le n\le N} \Gamma_*^n$. The finite element spaces defined in (14) are natural space-time generalizations of the "cut" finite element space defined in (5). We treat the Henry condition $[\![\beta u]\!]_\Gamma = 0$ using a natural space-time generalization of the Nitsche technique used in section 2.1.1. For this we need a suitable average across $\Gamma(t)$, denoted by $\{\!\{v\}\!\}_{\Gamma(t)} = \kappa_1(t) v|_{\Omega_1(t)} + \kappa_2(t) v|_{\Omega_2(t)}$. Take $t \in I_n$ and $T \in \mathscr{T}_n$ with $T_i := T \cap \Omega_i(t) \neq \emptyset$. We define the weights $\kappa_i(t) := |T_i|/|T|$. Note that those weights only depend on the *spatial* configuration at a given time t and there holds $\kappa_1(t) + \kappa_2(t) = 1$. Other choices for the averaging are possible, for instance the "Heaviside" choice that we also used in section 2.1.1 for the stationary case.

In the discontinuous Galerkin method we need jump terms across the end points of the time intervals $I_n = (t_{n-1}, t_n]$. We define $u_+^{n-1}(\cdot) := \lim_{\varepsilon\downarrow 0} u(\cdot, t_{n-1} + \varepsilon)$ and introduce the notation

$$v^n(x) := v(x,t_n), \quad [v]^n(x) := v_+^n(x) - v^n(x), \quad 0 \le n \le N-1, \quad \text{with } v^0(x) := 0.$$

On the cross sections $\Omega \times \{t_n\}$, $0 \le n \le N$, of Q we use a weighted L^2 scalar product

$$(u,v)_{0,t_n} := \int_\Omega \beta(\cdot,t_n) uv\, dx = \sum_{i=1}^2 \beta_i \int_{\Omega_i(t_n)} uv\, dx.$$

This scalar product is uniformly (w.r.t. n and N) equivalent to the standard scalar product in $L^2(\Omega)$. Note that we use a weighting with β in this scalar product, which is not reflected in the notation.

The notation introduced above is used to define a bilinear form $B(\cdot,\cdot)$, which consists of three parts, namely a term $a(\cdot,\cdot)$ that directly corresponds to the partial differential equation, a term $d(\cdot,\cdot)$ which weakly enforces continuity with respect to t at the time interval end points t_k, and a term $N_{\Gamma_*}(\cdot,\cdot)$ which enforces in a weak sense the Henry condition $[\![\beta u]\!]_{\Gamma_*} = 0$. These terms are defined per time slab Q^n, i.e. $a(\cdot,\cdot)$ is of the form $a(u,v) = \sum_{n=1}^N a^n(u,v)$ and similarly for the other two terms.

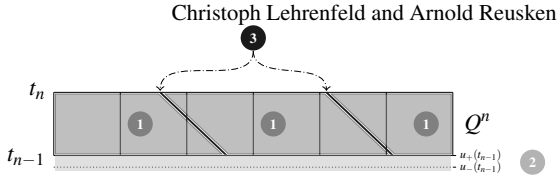

Fig. 4 Sketch of bilinear form contributions to space-time formulation for one time slab:
1. a^n: PDE (interior part),
2. d^n: temporal consistency,
3. $N^n_{\Gamma_*}$: interface conditions.

We now define the bilinear forms corresponding to each time slab Q^n, see also Fig. 4 for a sketch of these contributions. For sufficiently smooth u, v and $1 \leq n \leq N$ we define

$$a^n(u,v) := \sum_{i=1}^{2} \int_{Q_i^n} \big(\frac{\partial u_i}{\partial t} + \mathbf{w}\cdot\nabla u_i\big)\beta_i v_i + \alpha_i\beta_i \nabla u_i \cdot \nabla v_i \, dx\, dt, \tag{15a}$$

$$d^n(u,v) := ([u]^{n-1}, v_+^{n-1})_{0,t_{n-1}}, \tag{15b}$$

$$N^n_{\Gamma_*}(u,v) := \int_{t_{n-1}}^{t_n} N_h(t;u,v)\, dt, \tag{15c}$$

with the *spatial* Nitsche bilinear form $N_h(t;u,v)$ for a fixed time t defined analogously to (8b) and (8c) as

$$N_h(t;u,v) := N_h^c(t;u,v) + N_h^c(t;v,u) + N_h^s(t;u,v) \tag{15d}$$

$$N_h^c(t;u,v) := \int_{\Gamma(t)} \{\!\{-\alpha\nabla u\}\!\}_{\Gamma(t)} \cdot \mathbf{n}_{\Gamma(t)} \, [\![\beta v]\!]_{\Gamma(t)}\, ds, \tag{15e}$$

$$N_h^s(t;u,v) := \bar{\alpha}\frac{\lambda}{h} \int_{\Gamma(t)} [\![\beta u]\!]_{\Gamma(t)} [\![\beta v]\!]_{\Gamma(t)}\, ds, \quad \lambda \geq 0. \tag{15f}$$

Finally, we introduce a right-hand side functional given by

$$f^1(v) = (u_0, v_+^0)_{0,t_0} + \int_{Q^1} f\beta\, v\, dx\, dt, \quad f^n(v) = \int_{Q^n} f\beta\, v\, dx\, dt, \quad 2 \leq n \leq N,$$

where u_0 is the initial condition from (12c) and f the source term in (12a). Corresponding global (bi)linear forms are obtained by summing over the time slabs:

$$q(u,v) = \sum_{n=1}^{N} q^n(u,v), \text{ for } q \in \{a, d, N_{\Gamma_*}\}, \;\; f(v) = \sum_{n=1}^{N} f^n(v).$$

These bilinear forms and the functional f are well-defined on the space-time unfitted space W^{Γ_*}. The space-time unfitted FE discretization is defined as follows. Determine $u_h \in W^{\Gamma_*}$ such that

$$\begin{aligned} &B(u_h, v_h) = f(v_h) \quad \text{for all } \; v_h \in W^{\Gamma_*}, \\ &B(u_h, v_h) := a(u_h, v_h) + d(u_h, v_h) + N_{\Gamma_*}(u_h, v_h). \end{aligned} \tag{16}$$

Note that this formulation still allows to solve the space-time problem time slab by time slab.

Remark 4 (Quadrature in space-time). We assumed that no geometry errors are introduced in the discretization which implies the assumption that integration on the space-time subdomains Q_i^n and on the space-time interface Γ_* can be done exactly. In practice this assumption is not realistic and an approximation of the geometries is necessary to construct quadrature rules. While piecewise linear interface approximations, which have second order accuracy, are standard in up to *three* dimensions, cf. (among others) [27, Chapter 4], [36], [37, Chapter 5], the numerical integration on geometries resulting from piecewise linear interface reconstructions in *four* dimensions (three space and one time dimension) required new strategies. In [26] we presented decomposition rules which allow to extend the previously known strategies from lower dimensions to four dimensional geometries.

Remark 5 (Higher order methods). We comment on a generalization to a higher order method. On Q, instead of the bilinear space W as in (13), a higher order space-time finite element space can be defined in an obvious manner, cf. [53]. A corresponding higher order unfitted finite element space is then defined as in (14) and the higher order discretization is obtained by the variational problem (16) with W^{Γ_*} replaced by this higher order unfitted finite element space. We conclude that the method (16) has a straightforward generalization to a higher order method. From an implementation point of view there is an important difference between the bilinear method introduced above and a higher order method. In order to benefit from the higher order accuracy, one needs sufficiently accurate quadrature rules. For the case with an evolving interface such accurate approximations of the space-time integrals are difficult to realize. So far only second order quadrature rules have been dev eloped for implicitly described geometries in space-time, cf. Remark 4. An extension of the higher order accurate geometry handling as in section 2.1.1 to the space-time setting is a topic of current research.

2.2.2 Second order error bounds

Below in Theorem 2 we present a main result of the a priori error analysis of the unfitted space-time method. For this we first introduce some preliminaries. We need anisotropic Sobolev spaces. By $H^{k,l}(Q_1^n \cup Q_2^n)$ we denote the Sobolov space of functions on the domain $Q_1^n \cup Q_2^n$ with spatial partial derivatives up to degree k and temporal derivatives up to degree l in $L^2(Q_1^n \cup Q_2^n)$. The subscript 0 is used for the subspace of functions in $H^{k,l}(Q_1^n \cup Q_2^n)$ with zero value on $\partial\Omega \times (0,T)$ (in the trace sense), cf. [30] for details.

In order to derive second order bounds in the $L^2(\Omega(T))$ norm, we make use of duality arguments. This require regularity assumptions for the following homogenuous backward problem (with data $\hat{v}_T$):

$$-\frac{\partial \hat{v}}{\partial t} - \mathbf{w}\cdot\nabla\hat{v} - \operatorname{div}(\alpha\nabla\hat{v}) = 0 \quad \text{in } \Omega_i(t),\ i=1,2,\ t\in[0,T], \tag{17a}$$

$$[\![-\alpha\nabla\hat{v}]\!]_\Gamma\cdot\mathbf{n}_\Gamma = 0, \quad [\![\beta\hat{v}]\!]_\Gamma = 0 \quad \text{on } \Gamma, \tag{17b}$$

$$\hat{v}(\cdot,0) = \hat{v}_T \quad \text{in } \Omega_i(0),\ i=1,2, \tag{17c}$$

$$\hat{v}(\cdot,t) = 0 \quad \text{on } \partial\Omega,\ t\in[0,T]. \tag{17d}$$

The analysis in [30] uses the the assumption that the solution of this homogenuous backward problem has the regularity property $\|\hat{v}\|_{2,Q_1\cup Q_2} \leq c\|\hat{v}_T\|_{L^2(\Omega)}$ where $\|\cdot\|_{2,Q_1\cup Q_2}$ is the standard (isotropic) Sobolev norm. Based on this one can derive a second order error bound in the $L^2(\Omega)$ norm. In the analysis in [27] we replaced this assumption with the a more realistic regularity assumption $\|\hat{v}\|_{2,Q_1\cup Q_2} \leq c\|\hat{v}_T\|_{H^1(\Omega_1(T)\cup\Omega_2(T))}$ to arrive at the second order estimate given in the next theorem. The estimate gives a bound in a dual norm, the definition of which we repeat for functions $v\in L^2(\Omega)$:

$$\|v\|_{-1,T} := \sup_{w\in H^1_0(\Omega_1(T)\cup\Omega_2(T))} \frac{(v,w)_{0,T}}{\|w\|_{H^1(\Omega_1(T)\cup\Omega_2(T))}}.$$

Theorem 2. *Assume that* (12) *has a solution* $u\in H^{2,1}_0(Q_1\cup Q_2)$ *and* $u_h\in W^{\Gamma_*}$ *is the solution to* (16)*. Under the assumption that the homogeneous backward problem* (17) *has a solution* $\hat{v}\in H^2_0(Q_1\cup Q_2)$ *that has the regularity property* $\|\hat{v}\|_{2,Q_1\cup Q_2}\leq c\|\hat{v}_T\|_{H^1(\Omega_1(T)\cup\Omega_2(T))}$ *with a constant c independent of the initial data* $\hat{v}_T\in H^1(\Omega_1(T)\cup\Omega_2(T))$*, there holds the following bound for the discretization error* $u-u_h$*:*

$$\|(u-u_h)(\cdot,T)\|_{-1,T} \leq c(h^2+\Delta t^2)\|u\|_{2,Q_1\cup Q_2}. \tag{18}$$

Hence, the discretization error of this method is of second order, both with respect to the spatial and time mesh size, under reasonable regularity assumptions. In numerical experiments, cf. Section 2.2.3 below, we observe that the second order convergence also holds in the L^2-norm. We do not assume any CFL-type conditions on the mesh sizes. To our knowlegde there are no other Eulerian FE techniques which for this class of parabolic problems with an *evolving discontinuity* have a proven second order error bound.

2.2.3 Results of numerical experiments

We present results for a test problem also considered in [26]. In this problem a sphere is translated inside a cube with a time-dependent velocity. We give a summary of the setup and the results and refer to [26] for more details. The time interval is $[0,T]$ with $T=0.5$ and the domain is the cube $\Omega=[0,2]^3$. The sphere is initially centered around the origin $(0,0,0)$, has a radius $R=\frac{1}{3}$ and is translated by the time-dependent velocity field $\mathbf{w}$. Initial and boundary data are prescribed such that the solution takes the form

$$u(x,t) = \sin(k\pi t)\cdot U^m(\|x-q(t)\|),\ U^1(y) = a+by^2 \text{ and } U^2(y) = \cos(\pi y).$$

where $q(t) = (\frac{1}{4\pi}\sin(2\pi t),0,0)$ describes the center of the sphere at time t and a and b are chosen such that the interface conditions hold. We chose $(\alpha_1,\alpha_2) = (10,20)$ and $(\beta_1,\beta_2) = (2,1)$.

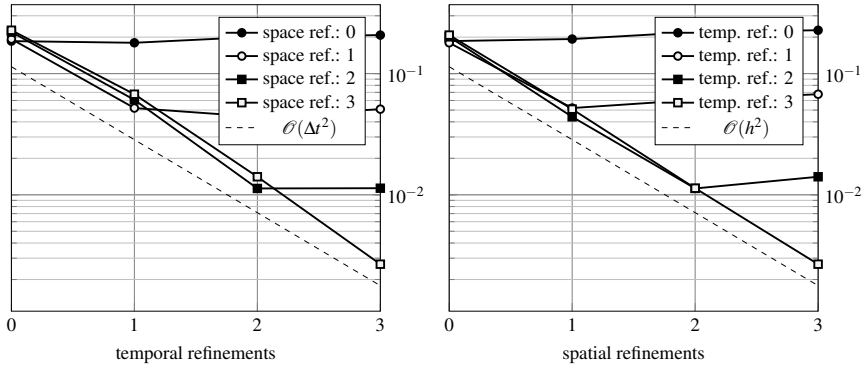

Fig. 5 Numerical results for the example in section 2.2.3. L^2 error at final time after repeated (uniform) refinements in time (left) and space (right).

In Fig. 5 we present results for the discretization error $\|u(\cdot,T)-u_h(\cdot,T)\|_{L^2(\Omega)}$. These results show a second order convergence of the error with respect to temporal and spatial refinements. We note that in further numerical studies we observed also third order convergence in time for many test cases as long as the quadrature error is sufficiently small. From the literature, e.g. [53], it is known that for *smooth* parabolic problems (i.e., without discontinuities) and with standard linear space-time FE spaces (no unfitted spaces, no Nitsche) the L^2 discretization error is of third order w.r.t. the time step.

3 Unfitted FEM for PDEs on surfaces

Below, in section 3.1 we first restrict to a model elliptic PDE, namely the Laplace-Beltrami equation on a *stationary* surface and then in section 3.2 extend the problem class to parabolic PDEs on evolving interfaces. In the past decade several finite element techniques for the discretization of (elliptic and parabolic) PDEs on a smooth (evolving) surface have been developed. For a recent overview we refer to [10]. These methods can be classified as follows. Firstly, the (evolving) *surface finite element method* (SFEM), developed by Dziuk and Elliott in a series of papers (cf. [10]), is based on an explicit triangulation Γ_h of Γ. On this triangulation one uses a standard linear finite element space. In case of an evolving surface the vertices of the triangulation are transported with the surface velocity field. Thus this method is

based on a Lagrangian approach. A second class of methods is based on an *extension of the PDE* (given on Γ) to a neighborhood of the surface. One then obtains a PDE in the volume, which can be discretized by standard FE techniques. The third class of methods consists of so-called *trace FEM* [40, 41, 39] in which one starts from a standard finite element space on an outer fixed volume mesh and then takes the trace on Γ of this space for the discretization of the surface PDE. This technique can also be applied to an evolving surface and results in a purely Eulerian approach. In this paper we restrict to the latter class of FE trace techniques, which can also be interpreted as an *unfitted* FEM: one starts from a standard finite element space on a (fixed) volume triangulation, which is not fitted to Γ, and differently from (5) or (14) one takes the trace of this space on Γ instead of on the subdomains (separated by the surface Γ).

Below, both for the case of a stationary and an evolving surface, we explain these unfitted finite element techniques (or trace FEM), discuss optimal theoretical error bounds and present results of a few numerical experiments, which illustrate the behavior of the methods. For the case of a stationary interface we briefly address the issue of the conditioning of the resulting discrete problem (Remark 6). The results in this section are based on [14, 39, 40, 41].

3.1 Model elliptic PDE on a stationary surface

Let $\Omega \subseteq \mathbb{R}^3$ be a polygonal domain and $\Gamma \subset \Omega$ a smooth, closed, connected 2D surface. Given $f \in H^{-1}(\Gamma)$, with $f(1) = 0$ we consider the following Laplace–Beltrami equation: Find $u \in H^1_*(\Gamma) := \{ v \in H^1(\Gamma) \mid \int_\Gamma v\, ds = 0 \}$ such that

$$a(u,v) = f(v) \quad \text{for all } v \in H^1_*(\Gamma) \tag{19}$$

with

$$a(u,v) = \int_\Gamma \nabla_\Gamma u \cdot \nabla_\Gamma v\, ds.$$

3.1.1 An unfitted FEM

We assume that the smooth interface Γ is the zero level of a smooth level set function ϕ, i.e., $\Gamma = \{ x \in \Omega \mid \phi(x) = 0 \}$. We will use *the same isoparametric mapping* Θ_h as in section 2.1.1. Hence we assume that we have available $\phi_h \in V_h^k$ (degree k) and $\hat{\phi}_h = I_1 \phi_h$ (degree 1), which are finite element approximations of ϕ (in a neighborhood of Γ). These finite element functions are used as input for the isoparametric mapping Θ_h. Recall the local volume triangulation $\mathscr{T}^\Gamma := \{T \in \mathscr{T}, T \cap \Gamma^{\text{lin}} \neq \emptyset\}$. The standard affine polynomial finite element space V_h^k is restricted to $\mathscr{T}^\Gamma$, i.e., $(V_h^k)_{|\Omega^\Gamma}$. To this space we apply the transformation Θ_h resulting in the isoparametric space

$$V_{h,\Theta}^k := \{ v_h \circ \Theta_h^{-1} \mid v_h \in (V_h^k)_{|\Omega^\Gamma} \}. \tag{20}$$

The *unfitted* finite element space that we use is the trace of this space:

$$V_{h,\Theta}^{\Gamma} := \mathrm{tr}|_{\Gamma_h}(V_{h,\Theta}^k), \qquad V_{h,\Theta}^{\Gamma,0} := \{\, v_h \in V_{h,\Theta}^{\Gamma} \mid \int_{\Gamma_h} v_h \, ds = 0 \,\}, \tag{21}$$

with $\Gamma_h := \Theta_h(\Gamma^{\mathrm{lin}})$. In the notation, we skip the polynomial degree k, and we use Γ to indicate that we *take the trace of the outer volume isoparametric space*. We introduce the bilinear form

$$a_h(u,v) := \int_{\Gamma_h} \nabla_{\Gamma_h} u \cdot \nabla_{\Gamma_h} v \, ds. \tag{22}$$

For the discrete problem we need a suitable extension of the data f to Γ_h, which is denoted by f_h. Specific choices for f_h are discussed in [47]. The discrete problem is as follows: Find $u_h \in V_{h,\Theta}^{\Gamma,0}$ such that

$$a_h(u_h, v_h) = \int_{\Gamma_h} f_h v_h \, dx \quad \text{for all } v_h \in V_{h,\Theta}^{\Gamma,0}. \tag{23}$$

Similar to the approach in Section 2.1.1, cf. (10), the implementation of the integrals in (23) is based on numerical integration rules with respect to Γ^{lin} and the transformation Θ_h. We illustrate this for the integral in (23). With $\tilde{u}_h = u_h \circ \Theta_h$, $\tilde{v}_h = v_h \circ \Theta_h \in V_h^{\Gamma}$, there holds

$$\int_{\Gamma_h} \nabla_{\Gamma_h} u_h \cdot \nabla_{\Gamma_h} v_h \, ds = \int_{\Gamma^{\mathrm{lin}}} \mathscr{J}_{\Gamma} \cdot \mathbf{P}_h D\Theta_h^{-T} \nabla \tilde{u}_h \cdot \; \mathbf{P}_h D\Theta_h^{-T} \nabla \tilde{v}_h \, ds,$$

with $\mathbf{P}_h = I - \mathbf{n}_h \mathbf{n}_h^T$ the tangential projection, $\mathbf{n}_h = \mathbf{N}/\|\mathbf{N}\|$ the unit-normal on Γ_h with $\mathbf{N} = (D\Theta_h)^{-T}\hat{\mathbf{n}}_h$ where $\hat{\mathbf{n}}_h = \nabla\hat{\phi}_h/\|\nabla\hat{\phi}_h\|$ is the normal with respect to Γ^{lin}, and $\mathscr{J}_{\Gamma} = \det(D\Phi_h) \cdot \|\mathbf{N}\|$. This means that we only need an accurate integration with respect to the low order geometry Γ^{lin} and the explicitly available mesh transformation $\Theta_h \in (V_h^k)^d$.

3.1.2 Optimal error bound

The following optimal H^1-norm error bound is derived in [14]. One part of the discretization error stems from the approximation of the data f on the discrete surface Γ_h. Let $\mu_h : \Gamma_h \to \mathbb{R}$ describe the ratio in measures between integrals on Γ and Γ_h, so that there holds $\int_{\Gamma_h} \mu_h \, u \circ \Phi \, ds = \int_{\Gamma} u \, ds$ for $u \in L^2(\Gamma)$ and $\Phi : \Gamma_h \to \Gamma$ the closest point mapping. One can show that $\|1 - \mu_h\|_{L^\infty(\Gamma_h)} \lesssim h^{k+1}$. With $f^e(x) = f(\Phi(x))$ the constant extension in normal direction, we have for $f \in L^2(\Gamma)$ and $v, f_h \in L^2(\Gamma_h)$:

$$\int_{\Gamma} f \; v \circ \Phi^{-1} \, ds - \int_{\Gamma_h} f_h \; v \, ds = \int_{\Gamma_h} (\mu_h f \circ \Phi - f_h) v \, ds = \int_{\Gamma_h} (\mu_h f^e - f_h) v \, ds,$$

which characterizes one part of the consistency error stemming from the geometry approximation. We introduce the data error quantity $\delta_f := \mu_h f^e - f_h$ on Γ_h.

Theorem 3. *Let $u \in H^{k+1}(\Gamma)$ be the solution of* (19) *and $u_h \in V_{h,\Theta}^{\Gamma,0}$ the solution of* (23)*. Assume that the data error satisfies $\|\delta_f\|_{L^2(\Gamma_h)} \lesssim h^{k+1}\|f\|_{L^2(\Gamma)}$. Then the following holds:*

$$\|u^e - u_h\|_{H^1(\Gamma_h)} \lesssim h^k \|u\|_{H^{k+1}(\Gamma)} + h^{k+1}\|f\|_{L^2(\Gamma)}. \tag{24}$$

Hence this method has the optimal h^k error bound in the H^1-norm, under optimal smoothness assumptions on u. An optimal L^2-norm error bound has not been derived, yet.

3.1.3 Results of numerical experiments

We consider an example taken from [16] and apply the discretization described above. The surface is a torus prescribed by the level set function ϕ, $\Gamma = \{x \in \Omega | \phi(x) = 0\}$ with

$$\phi(x) = \left(x_3^2 + \left(\left(x_1^2 + x_2^2\right)^{\frac{1}{2}} - R \right)^2 \right)^{\frac{1}{2}} - r, \quad R = 1, r = 0.6.$$

The solution is given as $u(x) = \sin(3\varphi)\cos(3\theta + \varphi)$ where (ϕ, θ) are the angles describing a surface parametrization, cf. [16] for details. The function f is chosen accordingly. u and f have mean value zero. We start from an initially mesh with mesh size $h \approx 0.1$ and repeatedly apply uniform refinements (at the interface).

In Fig. 6 we observe the convergence of the error $L^2(\Gamma_h)$ and the $H^1(\Gamma_h)$ semi norm. The rates are optimal, as predicted from the error bounds.

Remark 6 (Conditioning stiffness matrix). A disadvantage of the type of unfitted finite element method presented above is the fact that the stiffness matrix can be singular or extremely ill-conditioned. In particular this condition number depends not only on the mesh size h, but also on how the surface intersects the outer fixed triangulation $\mathscr{T}^\Gamma$. Recently, in [14] a general (i.e., applicable also to higher order FEM) stabilization technique has been introduced. In this method one uses a stabilization term of the form

$$s_h(u_h, v_h) = \rho_s \int_{\Omega_\Theta^\Gamma} \nabla u_h \cdot \mathbf{n}_h \, \nabla v_h \cdot \mathbf{n}_h \, ds,$$

with $\rho_s > 0$ a stabilization parameter, $\Omega_\Theta^\Gamma := \Theta_h(\Omega^\Gamma)$ (recall that Ω^Γ is the domain formed by all simplices that are intersected by Γ^{lin}) and $\mathbf{n}_h$ an approximation of the unit normal on $\Gamma_h = \Theta_h(\Gamma^{\mathrm{lin}})$ (cf. [14] for details). This stabilization term is added on the left-hand side in (23). It can be shown that with appropriately chosen ρ_s an optimal order error bound as in Theorem 3 still holds and the resulting stiffness

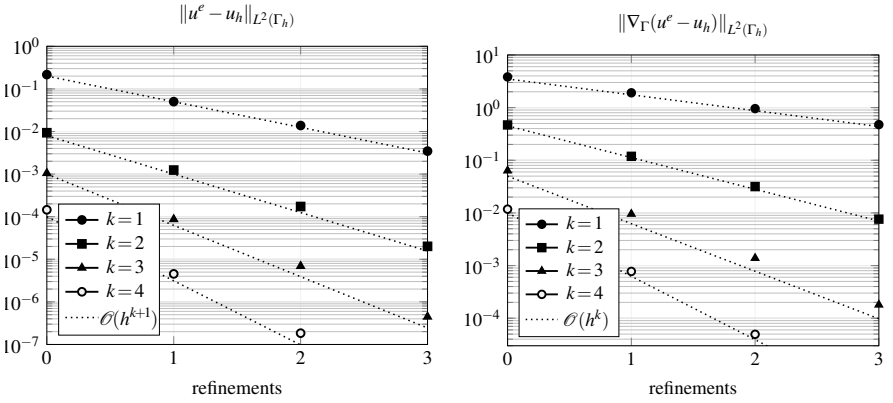

Fig. 6 Convergence history of the L^2 error under uniform refinement (left) and solution for a computation on the discrete surface Γ^{lin} (center) and Γ_h (right).

matrix has a condition number bounded by ch^{-2}, with a constant c independent of how the surface intersects the outer fixed triangulation.

3.2 Model parabolic PDE on an evolving surface

Consider a surface $\Gamma(t)$ passively advected by a *given* smooth velocity field $\mathbf{w} = \mathbf{w}(x,t)$, i.e. the normal velocity of $\Gamma(t)$ is given by $\mathbf{w}\cdot\mathbf{n}$, with $\mathbf{n}$ the unit normal on $\Gamma(t)$. We assume that for all $t \in [0,T]$, $\Gamma(t)$ is a hypersurface that is closed ($\partial\Gamma = \emptyset$), connected, oriented, and contained in a fixed domain $\Omega \subset \mathbb{R}^d$, $d = 2,3$. The convection-diffusion equation on the surface that we consider is given by:

$$\dot{u} + (\operatorname{div}_\Gamma \mathbf{w})u - \alpha_d \Delta_\Gamma u = f \qquad \text{on } \Gamma(t),\ t \in (0,T], \tag{25}$$

with a prescribed source term $f = f(x,t)$ and homogeneous initial condition $u(x,0) = u_0(x) = 0$ for $x \in \Gamma_0 := \Gamma(0)$. Here $\dot{u} = \frac{\partial u}{\partial t} + \mathbf{w}\cdot\nabla u$ denotes the material derivative, $\operatorname{div}_\Gamma := \operatorname{tr}\big((I - \mathbf{n}\mathbf{n}^T)\nabla\big)$ is the surface divergence and Δ_Γ is the Laplace-Beltrami operator, $\alpha_d > 0$ is the constant diffusion coefficient. If we take $f = 0$ and an initial condition $u_0 \neq 0$, this surface PDE is obtained from mass conservation of the scalar quantity u with a diffusive flux on $\Gamma(t)$ (cf. [22, 19]). A standard transformation to a homogeneous initial condition, which is convenient for a theoretical analysis, leads to (25). Several weak formulations of (25) are known in the literature, see [9, 19]. The most appropriate for our purposes is space-time formulation on the space-time manofold $\Gamma_* = \cup_{t\in[0,T]}\Gamma(t) \subset \mathbb{R}^{d+1}$ proposed in [41]. This well-posed space-time weak formulation, which we do not present here, forms the basis for the unfitted finite element presented in the next section.

3.2.1 An unfitted FEM

We use the same setting as in section 2.2.1. In particular, in the unfitted FEM that we present below we restrict ourselves to piecewise *bilinear* space-time functions (linear in space and linear in time). The space-time domain is denoted by $Q = \Omega \times (0,T] \subset \mathbb{R}^{d+1}$. A partitioning of the time interval is given by $0 = t_0 < t_1 < \ldots < t_N = T$, with (for simplicity) a uniform time step $\Delta t = T/N$. Corresponding to each time interval $I_n := (t_{n-1}, t_n]$ we assume a given shape regular simplicial triangulation $\mathscr{T}_n$ of the spatial domain Ω. In general this triangulation is *not fitted* to the interface $\Gamma(t)$. In the method we only need the local triangulation $\mathscr{T}_n^\Gamma$ (elements intersected by $\Gamma(t),\ t \in I_n$). In this section we assume that the (implicit) geometry $\Gamma(t)$ can be handled without introducing additional errors. In practice we need a geometry approximation, for which we use the same second order accurate approximation as briefly addressed in Remark 4. We use the same "outer" space-time finite element spaces W_n, W as in (13) and for the unfitted finite element space we take the *trace on* Γ_*:

$$W^{\Gamma_*} := W|_{\Gamma_*}. \tag{26}$$

For the definition of the finite element method we need some further notation. On $L^2(\Gamma_*)$ we use the scalar product $(v,w)_0 = \int_0^T \int_{\Gamma(t)} vw\, ds\, dt$. For $u \in W_n$, the one-sided limits $u_+^n = u_+(\cdot,t_n)$ (i.e., $t \downarrow t_n$) and $u_-^n = u_-(\cdot,t_n)$ (i.e., $t \uparrow t_n$) are well-defined. At t_0 and t_N only u_+^0 and u_-^N are defined. For $v \in W^{\Gamma_*}$, a jump operator is defined by $[v]^n = v_+^n - v_-^n$, $n = 1,\ldots,N-1$. For $n = 0$, we define $[v]^0 = v_+^0$. On the cross sections $\Gamma(t_n)$, $0 \le n \le N$, of Γ_* the L^2 scalar product is denoted by

$$(\psi,\phi)_{t_n} := \int_{\Gamma(t_n)} \psi\phi\, ds.$$

For the finite element discretization (which is based on a space-time weak formulation of (25)) we introduce the following bilinear forms:

$$a(u,v) = (\alpha_d \nabla_\Gamma u, \nabla_\Gamma v)_0 + (\mathrm{div}_\Gamma \mathbf{w}\, u, v)_0 \tag{27}$$

$$d^n(u,v) = ([u]^{n-1}, v_+^{n-1})_{t_{n-1}}, \quad d(u,v) = \sum_{n=1}^N d^n(u,v), \tag{28}$$

$$\langle \dot{u}, v\rangle_b = \sum_{n=1}^N \int_{t_{n-1}}^{t_n} \int_{\Gamma(t)} (\frac{\partial u}{\partial t} + \mathbf{w}\cdot\nabla u) v\, ds\, dt. \tag{29}$$

The unfitted finite element discretization of (25) is as follows: Find $u_h \in W^{\Gamma_*}$ such that

$$\langle \dot{u}_h, v_h\rangle_b + a(u_h,v_h) + d(u_h,v_h) = (f,v_h)_0 \quad \text{for all } \ v_h \in W^{\Gamma_*}. \tag{30}$$

Note that we use the same trial and test space W^{Γ_*} and that this method allows a time stepping procedure. One easily checks that this discretization is consistent in the sense that a solution of (25) satisfies the variational equation (30). Finally note that this method is a Eulerian method, based on a fixed (per time slab) outer triangu-

lation. For the implementation of the method one has to approximate the geometry and construct quadrature rules. So far, this has been done only for piecewise planar geometry approximations, cf. Remark 4.

3.2.2 Second order error bound

An error analysis of this method is presented in [38]. We outline a main result. Define $H = \{ v \in L^2(\Gamma_*) \mid \|\nabla_\Gamma v\|_{L^2(\Gamma_*)} < \infty \}$ endowed with the scalar product $(u,v)_H = (u,v)_0 + (\nabla_\Gamma u, \nabla_\Gamma v)_0$. Define the average $\bar{u}(t) := \int_{\Gamma(t)} u\, ds$. In the discretization error analysis we use a *consistent* stabilizing term involving the quantity $\bar{u}_h(t)$. More precisely, define

$$a_\sigma(u,v) := a(u,v) + \sigma \int_0^T \bar{u}(t)\bar{v}(t)\, dt, \quad \sigma \geq 0. \tag{31}$$

Instead of (30) we consider the stabilized version: Find $u_h \in W^{\Gamma_*}$ such that

$$\langle \dot{u}_h, v_h \rangle_b + a_\sigma(u_h, v_h) + d(u_h, v_h) = (f, v_h)_0 \quad \text{for all } \; v_h \in W^{\Gamma_*}. \tag{32}$$

Taking $\sigma > 0$ results in both a stabilizing effect and an improved discrete mass conservation property. Ellipticity estimates and error bounds are derived in the mesh-dependent norm:

$$|||u|||_h := \left(\|u_-^N\|_T^2 + \sum_{n=1}^N \|[u]^{n-1}\|_{t_{n-1}}^2 + \|u\|_H^2 \right)^{\frac{1}{2}}.$$

In the error analysis we need a condition which plays a similar role as the condition "$c - \frac{1}{2}\operatorname{div} b > 0$" used in standard analyses of variational formulations of the convection-diffusion equation $-\Delta u + b \cdot \nabla u + cu = f$ in an Euclidean domain $\Omega \subset \mathbb{R}^n$, cf. [49]. This condition is as follows: there exists a $c_0 > 0$ such that

$$\operatorname{div}_\Gamma \mathbf{w}(x,t) + \alpha_d c_F(t) \geq c_0 \quad \text{for all } \; x \in \Gamma(t),\ t \in [0,T]. \tag{33}$$

Here $c_F(t) > 0$ results from the Poincare inequality

$$\int_{\Gamma(t)} |\nabla_\Gamma u|^2\, ds \geq c_F(t) \int_{\Gamma(t)} (u - \frac{1}{|\Gamma(t)|}\bar{u})^2\, ds \quad \forall\, t \in [0,T],\ \ \forall\, u \in H. \tag{34}$$

A main result derived in [38] is given in the following theorem. To simplify the presentation, we assume that the time step Δt and the spatial mesh size parameter h have comparable size: $\Delta t \sim h$.

Theorem 4. *Assume* (33) *and take* $\sigma \geq \frac{\alpha_d}{2} \max\limits_{t\in[0,T]} \frac{c_F(t)}{|\Gamma(t)|}$, *where* $c_F(t)$ *is defined in* (34). *Then the ellipticity estimate*

$$\langle \dot{u}_h, u_h \rangle_b + a_\sigma(u_h, u_h) + d(u_h, u_h) \geq c_s |||u_h|||_h^2 \quad \textit{for all} \;\; u \in W^{\Gamma_*} \tag{35}$$

holds, with $c_s = \frac{1}{2}\min\{1, \alpha_d, c_0\}$ *and* c_0 *from* (33). *Let* $u \in H^2(\Gamma_*)$ *be the solution of* (25). *For the solution* $u_h \in W^{\Gamma_*}$ *of the discrete problem* (32) *the following error bound holds:*

$$|||u - u_h|||_h \leq ch\|u\|_{H^2(\Gamma_*)}.$$

A further main result derived in [38] is related to second order convergence. Denote by $\|\cdot\|_{-1}$ the norm dual to the $H_0^1(\Gamma_*)$ norm with respect to the L^2-duality. Under the conditions given in Theorem 4 and some further mild assumptions the error bound

$$\|u - u_h\|_{-1} \leq ch^2\|u\|_{H^2(\Gamma_*)}$$

holds. This second order convergence is derived in a norm weaker than the commonly considered $L^2(\Gamma_*)$ norm. The reason is that our arguments use isotropic polynomial interpolation error bounds on 4D space-time elements. Naturally, such bounds call for isotropic space-time H^2-regularity bounds for the solution. For our problem class such regularity is more restrictive than in an elliptic case, since the solution is generally less regular in time than in space. We can overcome this by measuring the error in the weaker $\|\cdot\|_{-1}$-norm.

3.2.3 Results of numerical experiments

For the results of experiments with the space-time unfitted FEM presented in Section 3.2.1 we refer to [41, 15]. In [41] results for the transport equation (25) on a smoothly evolving surface (e.g., shrinking sphere) are presented which clearly show a second order convergence (w.r.t. L^2-norm) both with respect to the space and the time mesh size. Furthermore, this convergence behavior occurs already on relatively coarse meshes. In [15] an example with a topological singularity is considered. For this example the assumptions we need in the error analysis are not satisfied. The evolving surface essentially consists of two disjoint spheres which approach each other and then merge. On this surface the transport equation (25) is considered. The space-time unfitted FEM presented in Section 3.2.1, cf. (30), is applied *without any modifications*. It turns out that despite the topological singularity the method yields satisfactory results, which indicates that this unfitted space-time FEM has very good robustness properties.

4 Applications to two-phase flows

In this section we present two examples of more advanced applications of the unfitted finite element techniques presented above. These applications are directly related to the main topics of the Priority Program 1506.

4.1 Mass transport in two-phase flow

We present numerical simulations of a dissolution process of oxygen from a rising (and deforming) air bubble into a water-glycerol solution. This example is treated in detail in [27]. We take a setting that has also been considered in [3, 25], [24, Chapter 9.8.3] and [42, Chapter 4.3.2]. Close to the bottom of a container filled with a homogeneuous water-glycerol mixture a 4*mm* spherical air bubble is placed. Due to buoyancy the bubble rises and deforms. After some time the rising of the bubble reaches a quasi-stationary state with an ellipsoidal shape. Initially the concentration of oxygen inside the fluid is assumed to be zero and a constant concentration u_0 is prescribed inside the bubble. During the rise of the bubble oxygen dissolves from the bubble to the fluid and a wake of oxygen follows the path of the bubble. Contour lines of the concentration for different times are depicted in Fig. 7. The material

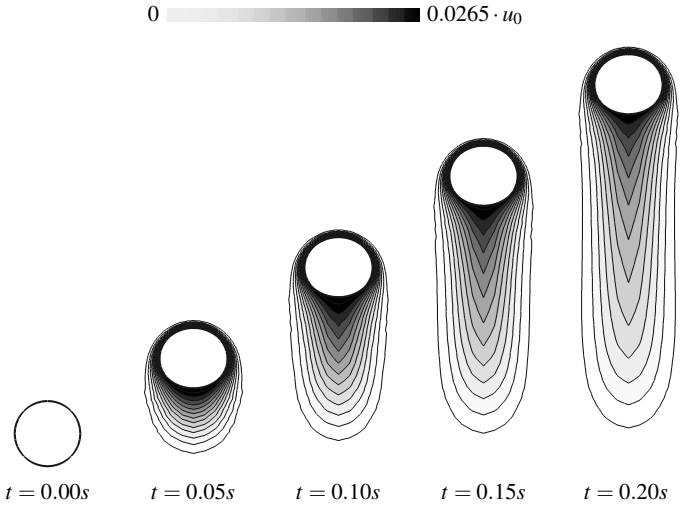

Fig. 7 Concentration contours in the fluid phase at several time for the dissolution process of oxygen from a rising air bubble in a water-glycerol mixture for Schmidt number $Sc = 10$.

parameters to this system are given in Table 1. While these parameters are realistic for the fluid dynamics, the diffusion coefficients are artificial in order to be able to prescribe a value for the Schmidt number $Sc = \frac{\mu}{\rho\alpha}$ in the liquid phase, $Sc = 10$. The simulation of the fluid dynamics is realized with the finite element software DROPS, cf. [17]. The software is based on a level set technique for interface capturing and (unfitted) modified $P_2 - P_1$ finite elements. We use adaptively refined tetrahedral grids close to the (evolving) interface and the wake of the bubble. We refer to [19] for details on the used model and its numerical treatment. The results obtained for the fluid dynamics have been validated against experimental data from [54]. For details we refer to [27, Section 5.4.1.1].

For the discretization of the mass transport problem we consider the unfitted space-time finite element method discussed in section 2.2 with bilinear functions

	liquid phase ($\Omega_2 = \Omega_L$)	disperse phase ($\Omega_1 = \Omega_B$)
density ρ $[kg/m^3]$	1205	1.122
dynamic viscosity μ $[Pas]$	0.075	1.824×10^{-5}
Henry weight β [1]	1	33
diffusion coeff. α $[m^2/s]$	$6.224 \times 10^{-5} \cdot Sc^{-1}$	1.916×10^{-5}
surface tension τ $[N/m]$	0.063	
init. bubble diameter d $[m]$	0.004	
gravity g $[m/s^2]$	9.81	

Table 1 Material parameters for the considered setting. The setting is the same as in [25, 3, 24].

(linear in space and linear in time) and a Nitsche stabilization parameter of $\lambda = 20$. At time $T = 0.2$ of the simulation we compare the concentration along straight lines

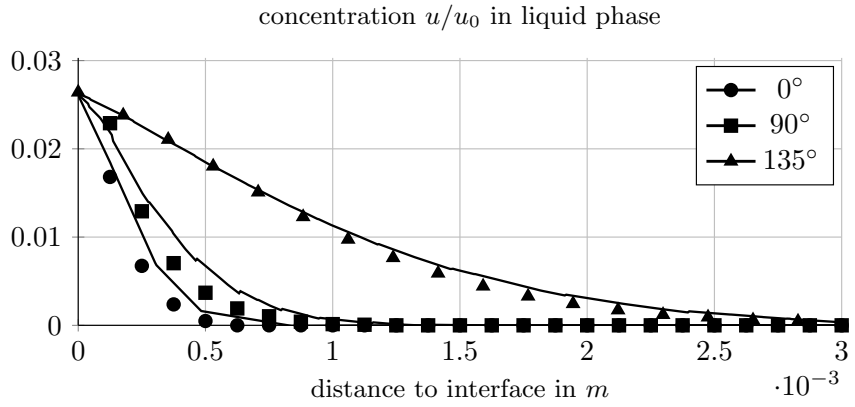

Fig. 8 Concentration layer profile in the liquid phase along lines of angles 0°, 90° and 135° computed with the space-time unfitted finite element method (lines) and comparison data (dots).

which are crossing the bubble center in Fig. 8. On the lines through the tip (0°), the equator (90°) and close to the wake (135°) we compare the concentration with simulated data from [42, Figure 9.35]. The results are in good agreement.

We can conclude that the numerical methods for the transport equations on evolving domains are robust and accurate even in these challenging realistic configurations.

4.2 Droplet breakup with surfactants

We present results of a numerical experiment for a two-phase flow problem with surfactants. This example is treated in detail in [55]. We briefly describe the model of this flow problem, the important model parameters and discuss a simulation result. For more information we refer to section 7.4 in [55]. The experiment is very similar to the one considered in [52]. In that paper, however, a *diffusive interface* model is

used, whereas we consider a *sharp interface* model. A spherical droplet with radius $r = 1$ is put in a rectangular box of dimensions 12(length)×4(width)×4(height), cf. Fig. 9, and exposed to a shear flow in the length direction with shear rate $\dot{\gamma} = 1$. The two fluids are Newtonian, modeled by the incompressible Navier-Stokes equations, and there is a surface tension force at the sharp interface. Dirichlet shear flow boundary conditions are imposed on the upper and lower boundaries. Periodic boundary conditions are imposed on all other boundaries. For the densities and viscosities we take $\rho_1 = \rho_2 = \mu_1 = \mu_2 = 1$. The Reynold's and Capillary numbers have values $Re = 0.4$, $Ca = 0.42$ (as in [52]). The surface tension coefficient for a clean interface has value $\tau_0 = 2.38$. We assume that there are insoluble surfactants (only) on the interface. The transport of these surfactants is modeled by the equation (25) with source term $f = 0$ and $\mathbf{w}$ resulting from the Navier-Stokes fluid dynamics model. For the effect of the surfactant concentration S on the surface tension coefficient the Langmuir model is used:

$$\frac{\tau(S)}{\tau_0} = 1 + \beta \ln(1 - \chi \frac{S}{S^*}),$$

with parameter values $\beta = 0.2$, $\chi = 0.1$, $S^* = 1.91 \times 10^{-5}$. The surfactant diffusion coefficient has value $\alpha_d = 0.1$.

We do not explain the components of the numerical solver used for the simulation of the fluid-dynamics, cf. the brief description in section 4.1. For further information we refer to [19]. The surfactant equation on the evolving interface is treated with the unfitted space-time FEM discussed in section 3.2.

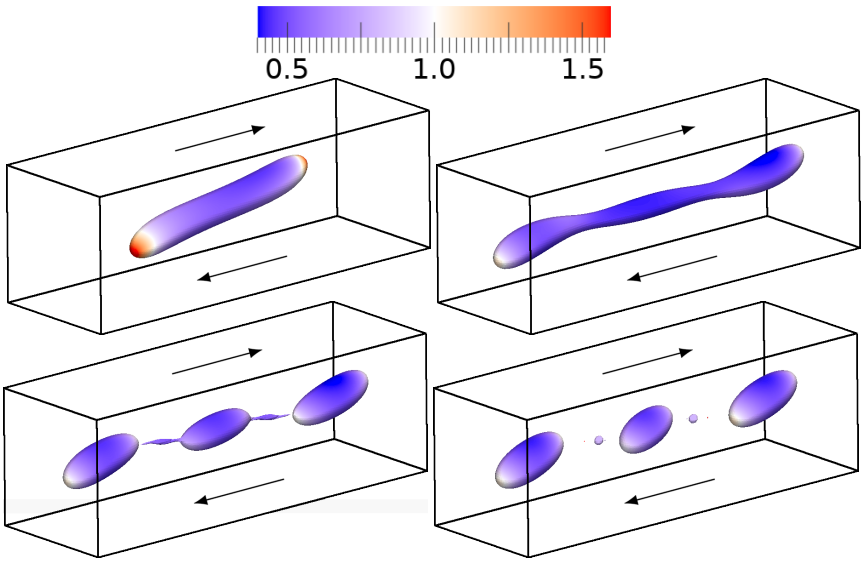

Fig. 9 Droplet in shear flow and surfactant concentration for $t = 10,\ 30,\ 37.5,\ 40$s.

In Fig. 9 we show a simulation result, which shows the interface evolution and surfactant concentration distribution. These (and further results in [55]) show a good agreement with simulation results from [52]. A comparison with a simulation for the clean droplet case shows that (as expected) due to the surfactants the droplet deforms more and breaks up earlier. The level set technique allows a robust handling of the droplet breakup. The unfitted space-time FEM is a robust discretization method for the surfactant transport equation. This method is exactly the same as the one presented in section 3.2, without any "tricky" modifications to deal with the droplet breakup.

5 Summary and outlook

We summarize the main new contributions obtained based on our research in the Priority Program 1506:

- We extended the combination of unfitted FEM with the Nitsche technique, already introduced in the literature for *stationary* interface problems, to problems with *evolving* interfaces. For this we developed and analyzed *space-time variants of unfitted FE and Nitsche methods* (section 2.2).
- We developed and analyzed a new method for obtaining *higher order accurate* approximations of implicitly described geometries. We applied this method to stationary interface problems (section 2.1) and to PDEs on stationary surfaces (section 3.1).
- The space-time unfitted FE technique is further developed for the discretization of PDEs on *evolving* surfaces (section 3.2).
- We developed a stabilization technique for convection dominated interface problems (remark 2).
- We developed a new optimal preconditoner for the efficient solution of a discretized stationary interface problem (remark 3).
- We applied these techniques not only to model problems, but also to more difficult applications in two-phase flow problems (section 4).

We briefly address a few topics, which we consider to be relevant for further research:

- So far the higher order unfitted FEM has been studied only for a *stationary* interface/surface. The extension of this approach to problems with *evolving* interfaces/surfaces is a subject of current research.
- For the unfitted FEMs treated in the sections 2.2 and 3.1 optimal order L^2-error bounds are not available, yet.
- Concerning stabilization techniques and preconditioners for the resulting discrete problems only very few results are known. More research is required to improve the efficiency of (iterative) solvers for these systems.
- The higher order methods presented in section 2.1 and 3.1 use different meshes, the original triangulation $\mathscr{T}$ and the curved mesh $\Theta_h(\mathscr{T})$, respectively, for the

definition of the level set function ϕ_h and a scalar field u. In cases where these quantities are coupled, i.e. where the level set (evolution) may depend on u the transfer of information from one mesh to the other has to be provided. Applying this in a proper way is another topic of current research.
- The performance of these relatively new (higher order) unfitted space-time FE techniques to challenging applications from e.g. two-phase flow problems should be investigated.
- We need a better understanding of the unfitted space-time method for PDEs on evolving surfaces with topological singularities.

Acknowledgements The authors gratefully acknowledge funding by the German Science Foundation (DFG) within the Priority Program (SPP) 1506 "Transport Processes at Fluidic Interfaces". Furthermore, we thank Jörg Grande for his contributions related to the research on surface PDEs.

References

1. P. Bastian and C. Engwer, *An unfitted finite element method using discontinuous Galerkin*, International Journal for Numerical Methods in Engineering, 79 (2009), pp. 1557–1576.
2. R. Becker, E. Burman, and P. Hansbo, *A Nitsche extended finite element method for incompressible elasticity with discontinuous modulus of elasticity*, Computer Methods in Applied Mechanics and Engineering, 198 (2009), pp. 3352 – 3360.
3. D. Bothe, M. Koebe, and H.-J. Warnecke, *VOF-simulations of the rise behavior of single air bubbles with oxygen transfer to the ambient liquid*, in Transport Phenomena with Moving Boundaries, F.-P. Schindler, ed., VDI-Verlag, Düsseldorf, 2004, pp. 134–146.
4. D. Bothe, M. Koebe, K. Wielage, J. Prüss, and H.-J. Warnecke, *Direct numerical simulation of mass transfer between rising gas bubbles and water*, in Bubbly Flows: Analysis, Modelling and Calculation, M. Sommerfeld, ed., Heat and Mass Transfer, Springer, 2004.
5. D. Bothe, M. Koebe, K. Wielage, and H.-J. Warnecke, *VOF-simulations of mass transfer from single bubbles and bubble chains rising in aqueous solutions*, in Proceedings 2003 ASME joint U.S.-European Fluids Eng. Conf., Honolulu, 2003, ASME. FEDSM2003-45155.
6. E. Burman, S. Claus, P. Hansbo, M. G. Larson, and A. Massing, *CutFEM: Discretizing geometry and partial differential equations*, International Journal for Numerical Methods in Engineering, (2014).
7. E. Burman and P. Hansbo, *Fictitious domain finite element methods using cut elements: II. a stabilized Nitsche method*, Applied Numerical Mathematics, 62 (2012), pp. 328–341.
8. T. Carraro and S. Wetterauer, *On the implementation of the eXtended finite element method (XFEM) for interface problems*, arXiv preprint arXiv:1507.04238, (2015).
9. G. Dziuk and C. Elliott, *Finite elements on evolving surfaces*, IMA J. Numer. Anal., 27 (2007), pp. 262–292.
10. ———, *Finite element methods for surface PDEs*, Acta Numerica, 22 (2013), pp. 289–396.
11. C. Engwer and F. Heimann, *Dune-UDG: a cut-cell framework for unfitted discontinuous Galerkin methods*, in Advances in DUNE, Springer, 2012, pp. 89–100.
12. A. Ern and J.-L. Guermond, *Finite element quasi-interpolation and best approximation*, arXiv preprint arXiv:1505.06931v2, (2015).
13. T.-P. Fries and T. Belytschko, *The extended/generalized finite element method: an overview of the method and its applications*, International Journal for Numerical Methods in Engineering, 84 (2010), pp. 253–304.

14. J. GRANDE, C. LEHRENFELD, AND A. REUSKEN, *Analysis of a high order Trace Finite Element Method for PDEs on level set surfaces*, in preparation, (2016).
15. J. GRANDE, M. OLSHANSKII, AND A. REUSKEN, *A space-time FEM for PDEs on evolving surfaces*, in Proceedings of the 11th World Congress on Computational Mechanics 2014, E. Onate, J. Oliver, and A. Huerta, eds., 2014.
16. J. GRANDE AND A. REUSKEN, *A higher order finite element method for partial differential equations on surfaces*, SIAM Journal on Numerical Analysis, 54 (2016), pp. 388–414.
17. S. GROSS ET AL., *DROPS package for simulation of two-phase flows*, 2015.
18. S. GROSS AND A. REUSKEN, *An extended pressure finite element space for two-phase incompressible flows*, J. Comput. Phys., 224 (2007), pp. 40–58.
19. S. GROSS AND A. REUSKEN, *Numerical Methods for Two-phase Incompressible Flows*, Springer, Heidelberg, 2011.
20. A. HANSBO AND P. HANSBO, *An unfitted finite element method, based on Nitsches method, for elliptic interface problems*, Computer Methods in Applied Mechanics and Engineering, 191 (2002), pp. 5537–5552.
21. M. ISHII, *Thermo-Fluid Dynamic Theory of Two-Phase Flow*, Eyrolles, Paris, 1975.
22. A. JAMES AND J. LOWENGRUB, *A surfactant-conserving volume-of-fluid method for interfacial flows with insoluble surfactant*, J. Comput. Phys., 201 (2004), pp. 685–722.
23. A. JOHANSSON AND M. G. LARSON, *A high order discontinuous Galerkin Nitsche method for elliptic problems with fictitious boundary*, Numerische Mathematik, 123 (2013), pp. 607–628.
24. M. KOEBE, *Numerische Simulation aufsteigender Blasen mit und ohne Stoffaustausch mittels der Volume of Fluid (VOF) Methode*, PhD thesis, Universität Paderborn, 2004.
25. M. KOEBE, D. BOTHE, AND H.-J. WARNECKE, *Direct numerical simulation of air bubbles in water/glycerol mixtures: shapes and velocity fields*, in Proceedings 2003 ASME joint U.S.-European Fluids Eng. Conf., Honolulu, 2003, ASME. FEDSM2003-451354.
26. C. LEHRENFELD, *The Nitsche XFEM-DG space-time method and its implementation in three space dimensions*, SIAM Journal on Scientific Computing, 37 (2015), pp. A245–A270.
27. C. LEHRENFELD, *On a Space-Time Extended Finite Element Method for the Solution of a Class of Two-Phase Mass Transport Problems*, PhD thesis, RWTH Aachen, February 2015.
28. C. LEHRENFELD, *High order unfitted finite element methods on level set domains using isoparametric mappings*, Computer Methods in Applied Mechanics and Engineering, 300 (2016), pp. 716–733.
29. C. LEHRENFELD AND A. REUSKEN, *Nitsche-XFEM with streamline diffusion stabilization for a two-phase mass transport problem*, SIAM Journal on Scientific, 34 (2012), pp. 2740–2759.
30. ———, *Analysis of a Nitsche-XFEM-DG discretization for a class of two-phase mass transport problems*, SIAM Journal on Numerical Analysis, 51 (2013), pp. 958–983.
31. ———, *Finite element techniques for the numerical simulation of two-phase flows with mass transport*, in Computational Methods for Complex Liquid-Fluid Interfaces, 2015, pp. 353–372.
32. ———, *Analysis of a high order unfitted finite element method for elliptic interface problems*, IGPM preprint 445, (2016).
33. ———, *L^2-estimates for a high order unfitted finite element method for elliptic interface problems*, arXiv preprint arXiv:1604.04529, (2016).
34. ———, *Optimal preconditioners for Nitsche-XFEM discretizations of interface problems*, Numerische Mathematik, first online (2016), pp. 1–20.
35. R. MASSJUNG, *An unfitted discontinuous Galerkin method applied to elliptic interface problems*, SIAM J. Numer. Anal., 50 (2012), pp. 3134–3162.
36. U. M. MAYER, A. GERSTENBERGER, AND W. A. WALL, *Interface handling for three-dimensional higher-order XFEM-computations in fluid–structure interaction*, International Journal for Numerical Methods in Engineering, 79 (2009), pp. 846–869.
37. T. A. NÆRLAND, *Geometry decomposition algorithms for the Nitsche method on unfitted geometries*, Master's thesis, University of Oslo, 2014.

38. M. OLSHANSKII AND A. REUSKEN, *Error analysis of a space-time finite element method for solving pdes on evolving surfaces*, SIAM Journal on Numerical Analysis, 52 (2014), pp. 2092–2120.
39. M. A. OLSHANSKII AND A. REUSKEN, *Error analysis of a space-time finite element method for solving pdes on evolving surfaces*, SIAM J. Numer. Anal., 52 (2014), pp. 2092–2120.
40. M. A. OLSHANSKII, A. REUSKEN, AND J. GRANDE, *A finite element method for elliptic equations on surfaces*, SIAM Journal on Numerical Analysis, 47 (2009), pp. 3339–3358.
41. M. A. OLSHANSKII, A. REUSKEN, AND X. XU, *An Eulerian space-time finite element method for diffusion problems on evolving surfaces*, SIAM J. Numer. Anal., 52 (2014), pp. 1354–1377.
42. A. ONEA, *Numerical simulation of mass transfer with and without first order chemical reaction in two-fluid flows*, PhD thesis, Forschungszentrum Karlsruhe, September 2007.
43. P. OSWALD, *On a BPX-preconditioner for $\mathbb{P}_1$ elements*, Computing, 51 (1993), pp. 125–133.
44. J. PARVIZIAN, A. DÜSTER, AND E. RANK, *Finite cell method*, Comput. Mech., 41 (2007), pp. 121–133.
45. Y. RENARD AND J. POMMIER, *GetFEM++, an open-source finite element library*, 2014.
46. A. REUSKEN, *Analysis of an extended pressure finite element space for two-phase incompressible flows*, Comput. Visual. Sci., 11 (2008), pp. 293–305.
47. ———, *Analysis of trace finite element methods for surface partial differential equations*, IMA Journal of Numerical Analysis, 11 (2015), pp. 1568–1590.
48. A. REUSKEN AND T. NGUYEN, *Nitsche's method for a transport problem in two-phase incompressible flows*, J. Fourier Anal. Appl., 15 (2009), pp. 663–683.
49. H.-G. ROOS, M. STYNES, AND L. TOBISKA, *Numerical Methods for Singularly Perturbed Differential Equations*, vol. 24 of Springer Series in Computational Mathematics, Springer, Berlin, Heidelberg, 1996.
50. S. SADHAL, P. AYYASWAMY, AND J. CHUNG, *Transport Phenomena with Droplets and Bubbles*, Springer, New York, 1997.
51. J. SLATTERY, L. SAGIS, AND E.-S. OH, *Interfacial Transport Phenomena*, Springer, New York, second ed., 2007.
52. K. TEIGEN, P. SONG, J. LOWENGRUB, AND A. VOIGT, *A diffuse-interface method for two-phase flows with soluble surfactants*, J. Comp. Phys., 230 (2011), pp. 375–393.
53. V. THOMEE, *Galerkin Finite Element Methods for Parabolic Problems*, Springer, Berlin, 1997.
54. M. WEGENER, *Der Einfluss der konzentrationsinduzierten Marangonikonvektion auf den instationären Impuls- und Stofftransport an Einzeltropfen*, PhD thesis, TU Berlin, September 2009.
55. Y. ZHANG, *Numerical Simulation of Two-phase Flows with Complex Interfaces*, PhD thesis, RWTH Aachen, 2015.